Microscopic Cascading Devices for Boosting Mucus Penetration in Oral Drug Delivery—Micromotors Nesting Inside Microcontainers

Maric, Tijana; Adamakis, Vaios; Zhang, Zhongyang; Milián-Guimerá, Carmen; Thamdrup, Lasse Højlund Eklund; Stamate, Eugen; Ghavami, Mahdi; Boisen, Anja

Published in:
Small

Link to article, DOI:
10.1002/smll.202206330

Publication date:
2023

Document Version
Publisher's PDF, also known as Version of record

NANO · MICRO small
www.small-journal.com

Microscopic Cascading Devices for Boosting Mucus Penetration in Oral Drug Delivery—Micromotors Nesting Inside Microcontainers

Tijana Maric, Vaios Adamakis, Zhongyang Zhang, Carmen Milián-Guimerá, Lasse Højlund Eklund Thamdrup, Eugen Stamate, Mahdi Ghavami, and Anja Boisen*

In the case of macromolecules and poorly permeable drugs, oral drug delivery features low bioavailability and low absorption across the intestinal wall. Intestinal absorption can be improved if the drug formulation could be transported close to the epithelium. To achieve this, a cascade delivery device comprising Magnesium-based Janus micromotors (MMs) nesting inside a microscale containers (MCs) has been conceptualized. The device aims at facilitating targeted drug delivery mediated by MMs that can lodge inside the intestinal mucosa. Loading MMs into MCs can potentially enhance drug absorption through increased proximity and unidirectional release. The MMs will be provided with optimal conditions for ejection into any residual mucus layer that the MCs have not penetrated. MMS confined inside MCs propel faster in the mucus environment as compared to non-confined MMs. Upon contact with a suitable fuel, the MM-loaded MC itself can also move. An in vitro study shows fast release profiles and linear motion properties in porcine intestinal mucus compared to more complex motion in aqueous media. The concept of dual-acting cascade devices holds great potential in applications where proximity to epithelium and deep mucus penetration are needed.

1. Introduction

Several drug administration routes have been developed and consolidated over the years.[1] They range from simple oral administration through traditional tablets or capsules, more invasive ones such as intravenous, intramuscular, and subcutaneous injections, all the way to complex implants such as insulin pumps.[2–4] While all of these routes have advantages and disadvantages, the pharmaceutical industry is constantly moving toward a more oral-focused administration approach due to minimum invasiveness and ease of use, which leads to higher patient compliance. While oral drug delivery has many advantages, it also features several challenges for macromolecules as well as poorly soluble and poorly permeable drugs.[5] First, it can be difficult to reach high drug concentration and bioavailability levels due to a poor absorption caused by multiple environmental challenges and unsuitable physiochemical properties of the drug.[6] Environmental challenges include: wide range of pH levels present in the gastrointestinal tract (GIT) (ranging from the very acidic stomach all the way to the mildly alkaline small intestine), digestive enzymes, bacteria present throughout the gut, multiple epithelial cell lines, and a thick protective mucus layer.[7–9] In order to offset the loss of the drug due to its poor absorption, a common practice is to use higher dose. This approach increases the cost of the final drug product in the case of an expensive active pharmaceutical ingredient (API) and can cause negative side effects in the GIT. Another

T. Maric, V. Adamakis, Z. Zhang, C. Milián-Guimerá, L. H. E. Thamdrup, M. Ghavami, A. Boisen
The Danish National Research Foundation and Villum Foundation's Center for Intelligent Drug Delivery and Sensing Using Microcontainers and Nanomechanics (IDUN)
Department of Health Technology
Technical University of Denmark
Ørsted Plads, Kgs. Lyngby 2800, Denmark
E-mail: tijma@dtu.dk

The ORCID identification number(s) for the author(s) of this article can be found under https://doi.org/10.1002/smll.202206330.

DOI: 10.1002/smll.202206330

T. Maric, V. Adamakis, Z. Zhang, C. Milián-Guimerá, L. H. E. Thamdrup, M. Ghavami, A. Boisen
Department of Health Technology
Technical University of Denmark
Kgs. Lyngby 2800, Denmark

E. Stamate
National Centre for Nano Fabrication and Characterization
Technical University of Denmark
Ørsteds Plads, Kgs. Lyngby 2800, Denmark

solution is to use drug delivery systems such as polymeric particles, liposomes, micromotors (MMs), and microcontainers (MCs) in order to protect the drug and increase its bioavailability.[10–12] Our group has developed both micro and macroscale devices (MCs, unfolding elastomeric foil and dynamic MMs) for oral drug delivery applications. These devices could potentially overcome major challenges associated with retention time, permeation, and drug degradation.[13–15] MCs can be made in various shapes and dimensions in order to perform optimally based on the target site and desired release profile.[16] They are usually featuring a concave hollow compartment in a non-permeable material.[17] Nielsen et al. used SU-8 MCs as a drug delivery system to improve bioavailability of the small molecule drug furosemide.[18] This finding was experimentally confirmed in a rat model whereby relative bioavailability increased twofold compared to a furosemide solution in capsules. MCs have also been employed as efficient vaccine, antibiotic, and probiotic carriers.[19–21] In contrast to passive MCs, MMs can autonomously propel themselves in certain environments and perform various functions leading to delivery of pharmaceutical compounds,[22] degradation of nitroaromatic explosives[23] and organic pollutants,[24] protein disaggregation,[25] photothermal therapy,[26] pH sensing,[27]vapor sensing,[28] and warfare agent removal.[29] The dynamic behavior allows MMs to become more readily engulfed in mucus and biofilms.[30–33] Their ability to propel is linked to energy conversion. MM motion can be caused by external stimuli or chemical reactions.[34–38] External stimuli-dependent MMs, use the energy provided via infrared light,[39] ultraviolet light,[40] magnetic force,[41] or ultrasound[42] to enable their motion. Self-propelled MMs, have been studied the most as these MMs are not dependent on external energy, instead taking advantage of bubble propulsion, self-electrophoresis, self-diffusiophoresis, or the Marangoni effect.[43] Over the past three decades, MMs have been widely explored for the loading and delivery of drugs.[44] Numerous types of materials have been used in the MM fabrication and many of them have demonstrated great potential to enhance mucus penetration and increase drug loading capability.[45,46] Great progress has been made using clarithromycin-MMs in vivo to treat bacterial disease in a mouse model.[47] Previous study investigated the effect of Mg-hydrogel MMs on tissue adherence efficiency, utilizing a unique suction-cup-like architecture.[48] It showed that through modifying the shape of MMs, adhesion properties can be modified, and a high loading capability of the Mg-hydrogel MMs can be achieved due to their porous structure.[48] Previously, Wang et al. used biocompatible PEDOT MMs (diameter of 5 μm and length of 25 μm) as microscale vehicles.[49] They successfully controlled the time that the MMs can travel in the GI tract just by adjusting the thickness of the polymer coating.

So far, MCs and MMs have been investigated separately for drug delivery and for their ability to attach to and embed inside mucus. Here, we for the first time demonstrate a combination of the two technologies resulting in a cascade device. By nesting MMs inside MCs it should be possible to protect the drug-carrying MMs until a targeted release site is reached. Comparing to the bare Mg/PEDOT/Au/Eudragit-MMs,[49] our system protects MMs all the way through the GI tract, enables MMs activation in a neutral environment (pH 7.4), and most importantly provides their unidirectional release in combination with close proximity to the epithelium. This trait is believed to enhance the bioavailability of drugs administered orally using MCs.[18] The MMs can hereby be protected as long as possible and be unidirectionally released to travel the final distance to the intestinal wall. Since the MMs are highly reactive when in contact with the surrounding media the result will be a cascading release event. They can penetrate partially through the mucus layer.[50]

Herein, we are presenting very detailed and novel experimental results related to the bulk production and associated characterization of enteric-coated SU-8 MCs loaded with MMs carrying the model drug paracetamol. The conceptual device is expected to combine the advantages of unidirectional drug release achieved by MCs orientation and the dynamic motion properties of MMs. In essence, the well-known dynamical movement of the MMs could ultimately further improve the bioavailability by bringing the loaded API even closer to the epithelium which has proven paramount for oral delivery/co-delivery of, for example, peptide drugs such as insulin.[51] Karshalev et al. used a pill to carry and protect Mg-based MMs through the GI tract. It was clearly proved that the encapsulation of the MMs does not have a negative effect on the motion behavior of the MMs.[52] Herein, we show that biocompatible magnesium-gold-MMs (Mg-Au-MMs) create self-propulsion and bubble generation via a chemical reaction at the exposed Mg surface of the MMs. The Mg reacts with a fuel supported by pitting and macro galvanic corrosion.[13] We coated paracetamol on the surface of Mg-Au-MMs, loaded the MMs inside the MC cavity, and then deposited an enteric lid composed of Eudragit L100. The studied devices are hereby-abbreviated magnesium-gold-paracetamol-MMs (Mg-Au-Para-MMs), and magnesium-gold-paracetamol-MMs loaded into MCs (Mg-Au-Para-MM-MCs). After preparation, we confirmed the presence of drug on the MMs confined inside the MCs and non-confined MMs using coherent anti-Stokes Raman scattering (CARS) microscopy. Even though the pioneering application of CARS microscopy for evaluating drug distribution on MMs was introduced just recently,[13] the current manuscript provides further experimental results that clearly establishes CARS as a feasible, robust, and highly attractive platform for conducting fundamental research on novel microscale devices for enhanced drug delivery via the oral route.

Besides outlining a sound strategy for producing the MM-loaded MCs we are also taking an in-depth experimental look at the dynamics associated with the triggered release of the MMs from the MCs. In this regard we are, to the best of our knowledge, presenting entirely new empirical data probing into the feasibility associated with oral drug delivery mediated by MMs hosted in microscale compartments. The propulsion ability of MMs was not affected by their storage in the cavity of the MCs. We have proved additional movement of the MCs filled with MMs that could potentially be explored as a means to ensure further mucus embedment. An in vitro drug release study in neutral and acidic medium, demonstrated time-dependent drug release profile as a function Eudragit L100 thickness. We showed how the cascade device works as an effective drug protective tool and pH-dependent release device. In addition, we also presented ex vivo data of Mg-based MMs during bubble propelled translation in porcine mucus. Here, we identified a

desired linear movement of the MMs inside mucus and travel ranges of ≈30 μm s^{-1} were achieved. These results are particularly important in terms of generating a more profound empirical understanding of how MMs move in fluids with clinically relevant rheological properties.

2. Results and Discussion

Herein, we introduce cascade microdevices for efficient cargo protection and enhanced penetration through the porcine mucus (**Scheme 1**). The proposed device is composed of two parts: a passive MC and dynamic MMs dispersed in the concave cylindrical compartment of the MC. The Mg-Au-Para MMs have been used as a model drug delivery system in this study. The MM fabrication steps include deposition of Mg microparticles with a thick Au layer (20 nm) and loading with paracetamol (Scheme 1b). A 2-inch TORUS magnetron sputtering cathode was used to achieve a uniform Au coating on one Mg hemisphere while the other hemisphere remained uncoated. These MMs displayed directional motion after contact with a fuel due to the structural asymmetry. The Au layer has been employed as a shell scaffold that leads to consistent MM propulsion. We chose paracetamol as the model drug as it is highly water soluble so it could be easily released from microdevices, and it has high bioavailability in the intestine (70–90%) and no absorption in the stomach.[53]

The cascade microdevices were prepared following the procedure displayed in Scheme 1a. Briefly, cylindrical MCs were fabricated by UV curing SU-8 on metal coated silicon substrates (more information in Experimental Section). Each MCs chip was manually loaded (Scheme 1c) with Mg-Au-Para-MMs using a polydimethylsiloxane (PDMS) mask.[54] Following the loading step, the filled MCs were coated with Eudragit L100 and stored until needed for measurements. The created cascade microdevices are highly biocompatible; the biocompatibility of SU-8 MCs has been demonstrated before.[55] It is widely known that Mg does not cause toxicological tissue response,[56] while Au is an accepted material in drug delivery. For example, Au nanoparticles have shown great promise in different biomedical application such as photothermal therapy,[57] in vitro diagnostics,[58] fast detection of food-borne pathogens in preventive medicine,[59] and stabilization of liposomes' efficiency as drug delivery carriers[60]

We first characterized Mg-based MMs and MCs, separately, to examine their composition and morphology. For this, a series of characterization techniques were applied. These included scanning electron microscopy (SEM), energy dispersive X-ray spectroscopy (EDX), and CARS microscopy.

Figure 1a shows SEM images of bare Mg microparticles. Magnified areas of SEM images are presented in Figure 1a as well. The Mg microparticles have a spherical shape with an average diameter of 24 ± 3 μm. Upon coating with Au on one hemisphere, there is a paradigm shift in the structure and morphology of the Mg microparticles, from plain spherical particles to Janus particles (Figure 1b). A thin film with a rougher texture is visible on one half of the Mg microparticles confirming the presence of an outer coat. The diameter of the Mg-Au-MMs does not change when sputtered with 20 nm of Au. Energy-dispersive X-ray mapping is shown in Figure 1c. A Mg signal is present over the entire particle (green color) while a trace amount of Au (red color) is detected only in one hemisphere of the microparticle. This confirms that a Janus structure is obtained by asymmetrical coating of an Au layer on the Mg microsphere. The Au-Mg MMs loaded with paracetamol drug show increased roughness and small spots across the MM surface (Figure 1d). The loaded MMs demonstrate homogeneously distributed drug over the MM surface without any visible degradation. The paracetamol was found to have bounded to both Mg and Au by physical adsorption through weak van der Waals forces. The chemical structure of paracetamol is shown in Figure 1e.

To achieve the most efficient MM protection from the harsh environment in the GIT and to ensure unidirectional release of loaded MMs toward the epithelium, we placed MMs in MCs.[61] Fabricated MCs before and after loading with MMs were visualized with SEM and are displayed in **Figure 2**. The left panels of Figure 2 show SEM images of single MCs, while the right panels show multiple MCs. Figure 2a displays the cylindrical shape and uniform size of empty MCs placed on a square MC chip. MCs are arranged in a 2D array on quadratic silicon chips. The average outer MC diameter is 330 μm, the inner diameter

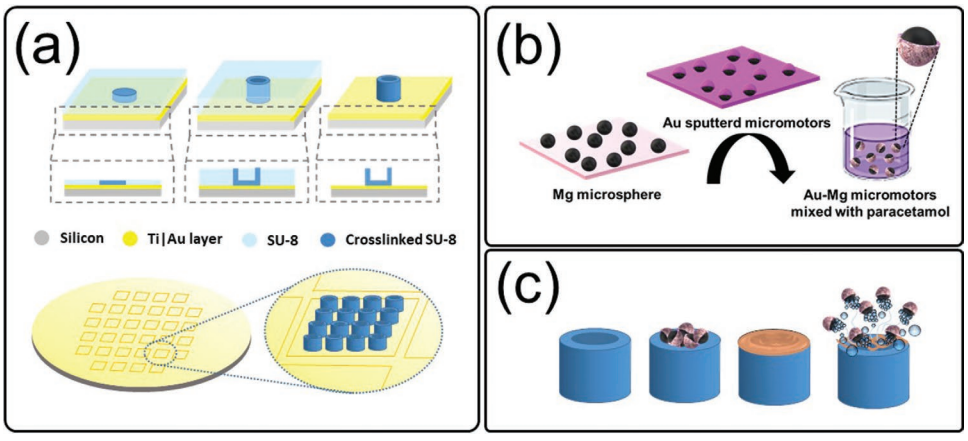

Scheme 1. Schematic of cascade microdevices preparation. a) MCs preparation. b) Preparation of Mg-Au-Para-MMs. c) Loading of Mg-Au-Para-MMs on MCs and coating with Eudragit L100 enteric coating.

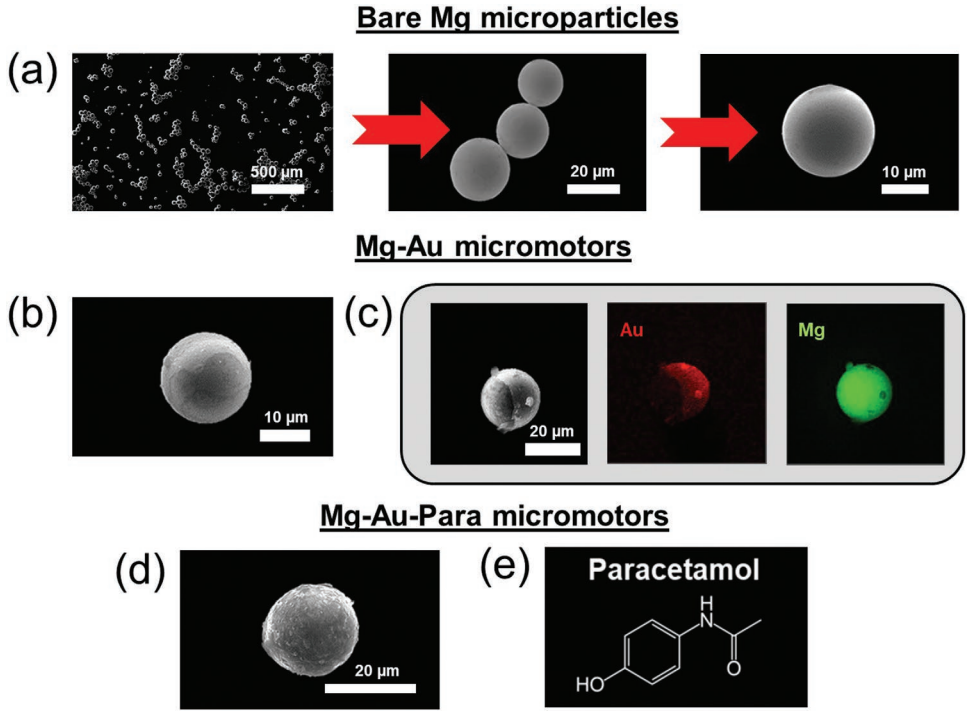

Figure 1. SEM of a) bare Mg microparticles, and b) Mg-Au-MMs. c) SEM of Mg-Au-MM and corresponding energy-dispersive X-ray (EDX) images illustrating the distribution of Au (red) and Mg (green) in the MM, and d) Mg-Au-Para-MMs. e) Chemical structure of paracetamol.

is 230 µm, and the overall height is 240 µm. The monodispersity of the MCs is essential for ensuring a homogenous compartment volume available for cargo loading. Before loading with Mg-Au-Para-MMs, a PDMS shadow mask was made on the MC chips following a previously outlined procedure.[54] The free spaces between the MCs were covered with a PDMS mask to minimize the MM accumulation between MCs and to decrease wastage (Figure 2b). Figure 2c displays MCs successfully filled with the Mg-Au-Para-MMs in the presence of the PDMS mask. Subsequently, the PDMS mask was peeled off using tweezers. The resulting MMs-loaded MCs are illustrated in Figure 2d. Finally, the loaded MCs were sealed with a pH sensitive Eudragit L100 polymer coating using an ultrasonic spray coater. The coating was performed to protect the MMs inside the cavity but also to achieve targeted drug release and enhanced drug retention until the desired environment was reached.

The Eudragit layer has a consistent thickness of 20 µm over the whole chip area (Figure 2e).

The drug presence was traced by CARS microscopy as shown in **Figure 3**a. This analysis was implemented to prove that paracetamol was successfully attached onto the surface of Janus MMs. To generate the CARS signals, two near-infrared laser beams were employed, which enable deeper imaging and minimize auto-fluorescence. First, we performed a lambda excitation scan on pure paracetamol (Figure 3b) to find the correct wavelength for imaging, while the CARS 1200S (top image) and CARS 2000S (bottom image) filters were, respectively, used to cover the Raman shift range from 1200 to 2000 cm^{-1} and above 2000 cm^{-1}. Based on the presented spectrums (Figure 3b), paracetamol manifests two strong signals found at 1610.26 and 3051.4 cm^{-1}, both can be further used in the experiments to visualize paracetamol. All performed experimental conditions are recorded in Table S1, Supporting Information.

Subsequently, the Mg-Au-MMs were imaged with a CARS microscope. They showed no CARS signal, as expected, but they showed fluorescence signal originating from the Au when using the white light laser source at 556 nm and the photo-multiplier tube detector (PMT1). Figure 3c shows the signal distribution of the Au from the Mg-Au-MM. Once the Au signal had been determined, the CARS imaging was used to confirm the presence of paracetamol on the Mg-Au-Par MMs. As seen in Figure 3d, two signals are collected, one enclosing a paracetamol (red) and one enclosing Au (green). The Au layer shows a two-photon excitation fluorescence (TPFE) signal triggered by the pump laser and is detected by using the second harmonic generation detectors. The paracetamol shows a strong CARS signal at 3051.4 cm^{-1} observed by CARS detectors. The composite image is presented as an overlay of CARS and TPFE signals, which suggests that not only the Au layer is present on the Mg-core, but also the paracetamol. We also provided chemical mapping of Mg-Au-Para-MM-MCs by CARS microscopy (Figure 3e). The paracetamol is depicted in red, while the Au is depicted in green. As seen in Figure 3e, the CARS signal associated with the drug comes from the MC cavity. This indicates that the drug is indeed encapsulated within the MCs and not in the voids between them. The green overexposure of the background is caused by the Au present on the MC chip due to the before mentioned release layer composed of 5 nm Ti and 20 nm Au. Last, the overlaid images of paracetamol and Au on a single and multiple MCs are presented. This proves that the loading was successful and that the MMs are present only within the MCs.

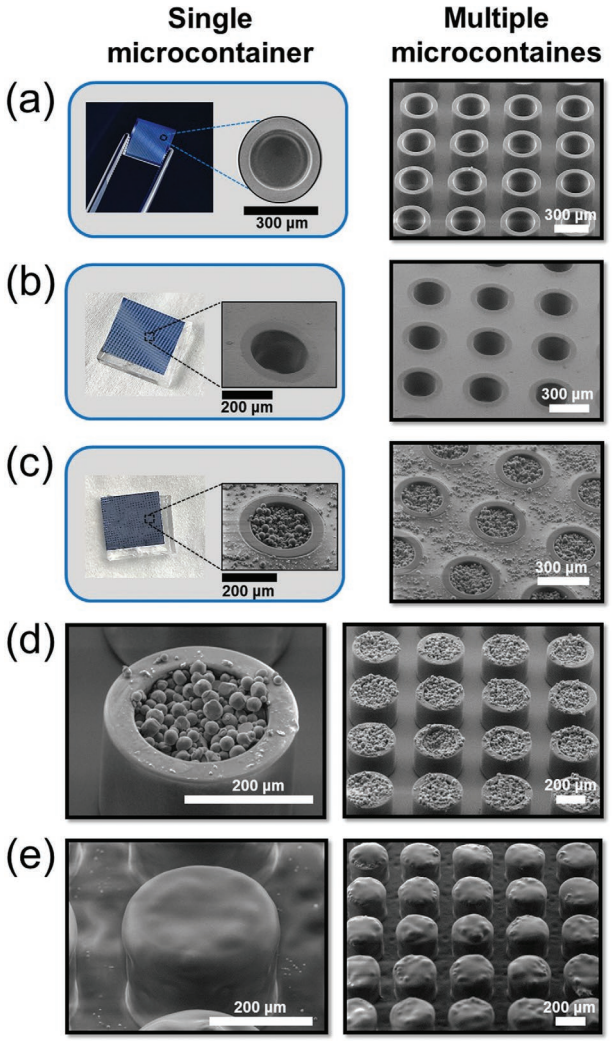

Figure 2. SEMs of single MC (left) and multiple MCs (right) during the MM loading procedure. a) Empty MCs. b) MC chip after applying PDMS shadow mask. c) Loaded MC with PDMS mask still present. d) Loaded MC after PDMS mask removal. e) MC after coating with Eudragit L100 polymer coating.

Subsequently, we determined the average size and size distribution of the Mg-Au-MMs, by using an optical microscope alongside NIS Elements Software. 100 MMs were measured and divided into six size groups: 15–18, 18–21, 21–24, 24–27, 27–30, and 30–33 µm. As shown in **Figure 4**a, most of the MMs have a diameter between 21 and 27 µm with their mean diameter being 24 µm and a standard deviation of 3 µm. However, there were some outliers, such as the largest and smallest MMs with diameters of 31 and 18 µm, respectively. It is important to mention that the addition of the Au layer did not influence the size distribution in a significant way as it only added 20 nm to the MMs' diameter. This is a small proportion with respect to the MMs' total diameter. These size variations between MMs can result in differences in the MM lifetime[62] and velocity[63] as well as drug loading ability.

As the use of MMs stems from their ability to self-propel and move in various media, a motion study was conducted to measure their velocity under different conditions. In general, Mg cores can easily react with fuels, such as water and acids, producing H_2 bubbles. However, alongside the H_2 bubbles, a passivation layer of magnesium hydroxide (Mg(OH)2) is formed which inhibits further reaction of the MMs with the fuel and leads to loss of their propulsion functionality.[64] Depending on the fuel, there are diverse ways to overcome this challenge. If the fuel of choice is NaCl, the chloride anions (Cl^-) promote pitting corrosion of the passivation layer in aqueous solutions. Moreover, when an Au layer is used during the fabrication of these Janus MMs, macrogalvanic corrosion of the passivation layer also occurs. Both pitting corrosion and macrogalvanic corrosion result in a shedding of the passivation layer, prolonging the MM's propulsion time.[62] If the fuel of choice is $NaHCO_3$, the passivation layer reacts with sodium bicarbonate and thus it can be removed easily.[65] We now studied whether paracetamol loading influences the propulsion of the MMs, and as such, we measured the velocity of both Mg-Au and Mg-Au-Par-MMs in the $NaHCO_3$ and NaCl fuels, separately. Thus, the movement of 20 MMs of each type was recorded in both fuels and their velocities were calculated (Figure 4b). The final concentrations of the NaCl, $NaHCO_3$, and Triton X-100 are 2, 0.67 M, and 0.34 wt%, respectively. The Mg-Au-Par-MMs in NaCl (77 ± 21.9 µm s^{-1}) showed the highest average velocity. This is an impressive increase of 39.6% compared to the average velocities of Mg-Au-MMs in NaCl (55.15 ± 13.7 µm s^{-1}). Mg-Au-MMs in $NaHCO_3$ feature an average velocity of 70.1 ± 16.2 µm s^{-1}, while the Mg-Au-Par-MMs in $NaHCO_3$ has an average velocity of 65.3 ± 25.1 µm s^{-1}. Mg-Au-MMs in $NaHCO_3$ feature a 27.1% higher average velocity than Mg-Au-MMs in NaCl. Mg-Au-Par-MMs in NaCl are 17.9% faster than Mg-Au-Par-MMs in $NaHCO_3$. To find the significance of these differences, statistical analysis by performing a one-tailed *t*-test with a significance level of $p < 0.05$ was conducted. It shows a significant difference between the average velocities of Mg-Au and Mg-Au-Par-MMs in NaCl ($p = 0.0004$) suggesting that the presence of the drug increases the velocity only when NaCl is used as the fuel and not when $NaHCO_3$ ($p = 0.2787$) is used. Moreover, a statistically significant difference ($p = 0002$) was found between the Mg-Au-MMs in the two different fuels while no such difference was found between the Mg-Au-Par-MMs under similar conditions ($p = 0.1749$). Therefore, it is safe to assume that both the fuel and the drug loading can potentially influence the velocity of MMs. One explanation would be that paracetamol is interacting with the Mg passivation layer shedding mechanisms of the MMs in NaCl, resulting in a beneficial effect that increases propulsion. Such an effect is unlikely to take place in $NaHCO_3$, as paracetamol here is seen to have no considerable influence on the velocity.

Figure 4d shows the movement of the MMs in a time span of 4 s. All four studied cases featured near-linear trajectories as can be seen in Figure 4d. Some MMs moved along circular trajectories (not presented here) and some moved along the both-linear and circular trajectories at different time points. A Reynolds number slightly below 10^{-3} leads to mostly linear trajectories, with a lower chance of circular trajectories, which could explain the presented data.[66] The tracking pictures are in correlation with calculated velocities of MMs; MMs with longer trajectories show faster motion for the same time interval.

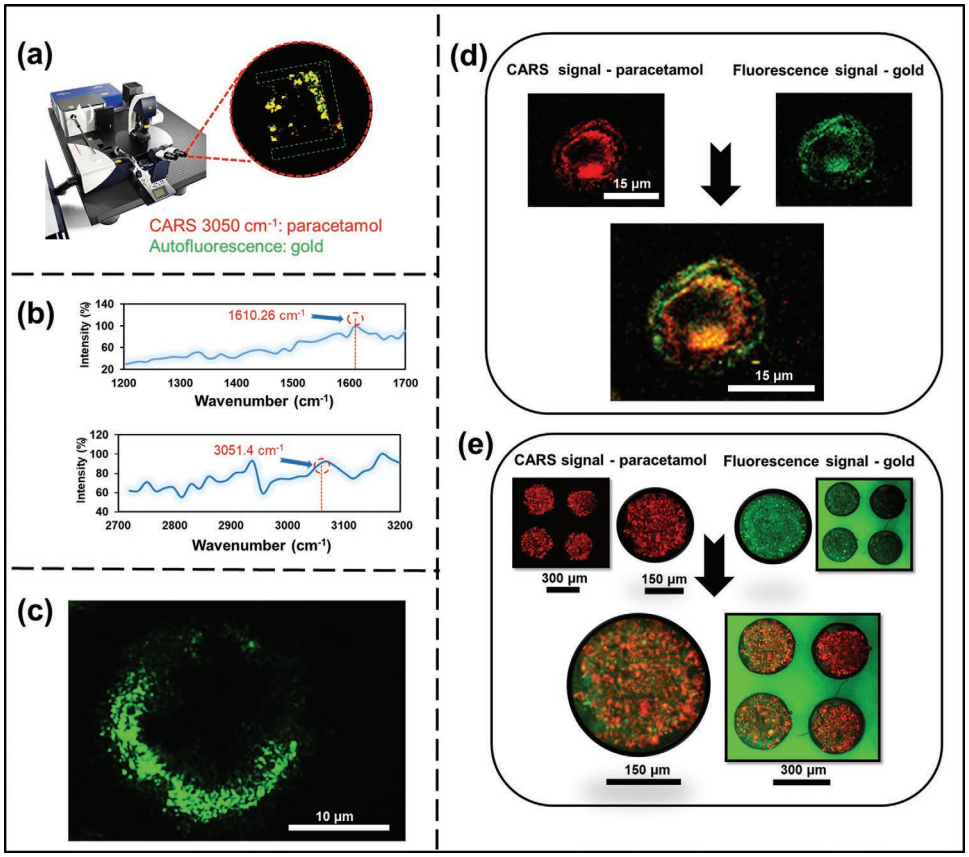

Figure 3. a) Schematic overview of the coherent anti-Stokes Raman scattering (CARS) microscopy system. b) CARS spectrum of paracetamol when using the CARS 1200S (top image) and CARS 2000S (bottom image) filters and performing the lambda excitation scan. Blue arrows highlight 1610.26 and 3051.4 cm^{-1} high intensity spots, respectively, used for paracetamol determination. c) Fluorescence of Au present on an Mg-Au-MM. d) CARS imaging of paracetamol in combination with two-photon excitation fluorescence (TPEF) signals from Au on a single Mg-Au-Para-MM. e) Combined CARS and TPFE imaging of MCs after loading with Mg-Au-Para-MMs.

An important aspect of MMs is their lifetime, which is the amount of time they can generate bubbles and self-propel when being exposed to the fuel. Therefore, the Mg-Au and the Mg-Au-Par-MMs were observed under microscope and their lifetimes were measured and compared. Two types of fuels, $NaHCO_3$ and NaCl, 0.67 and 2 M, respectively, were used to accomplish this, with the addition of the surfactant 0.34 wt% Triton X-100. These conditions were the ones that provided the best MM propulsion and that is why they were chosen. According to the results, which can be seen in Figure 4c, the measured lifetimes fall well into the 1–6 min expected range.[65] Statistical analysis of p-values with a significance level of $p < 0.05$ showed no significant difference between Mg-Au and Mg-Au-Par-MMs in neither $NaHCO_3$ ($p = 0.0733$) nor NaCl ($p = 0.0563$). Therefore, according to these results it is safe to assume that the presence of the drug on the MMs does not influence their lifetime. Regarding the fuel, there was no significant difference between the Mg-Au-Par-MMs ($p = 0.1850$). However, a significant difference was found ($p = 0.0246$) between the Mg-Au-MMs in the two fuels. The Mg-Au-MMs remove their passivation layer through different mechanisms in the two fuels and this is likely to have an influence on the lifetime.

An interesting aspect of the current study is the interaction and behavior of MCs in contact with a fuel. To study this, we loaded MCs with Mg-Au-Para-MM and coated them with Kollicoat protect polymer. It dissolves in water and is unaffected by differences in the solution's pH levels thus it is a suitable choice when targeting an immediate release. SEM images of MCs coated with Kollicoat protect polymer are presented in Figure S1, Supporting Information. 2 M NaCl and 0.34 wt% Triton X-100 have been used as a fuel in these experiments. During the first few seconds, no bubbling took place as the MC coating hindered the fuel from reaching the MMs. However, after 1 min, it was clear that the fuel had entered the MCs due to the extensive bubble formation, which is evident in **Figure 5**. In Figure 5a,b, it is apparent that bubble formation occurs at the top of MCs. Apart from bubble formation, several MMs left the MC within the 1st min; this is displayed by a tracking path in Figure 5b. After ≈1 min, MCs start self-moving with an average velocity of 17 µm s^{-1}. The Mg part of MMs inside the MC's well reacts with fuel and generates bubbles at the top part of MCs, which propels the MCs in the opposite direction using bubble-propulsion mechanism (Video S1, Supporting Information, and Figure 5c). We estimate that ≈70% of the Mg-Au-Para-MMs have escaped the MC after 25 min (Figure S2, Supporting Information). At the same time, the Mg-Au-Para-MMs release from the MC's and start their own self-motion. This dual MC-MM motion might be an additional

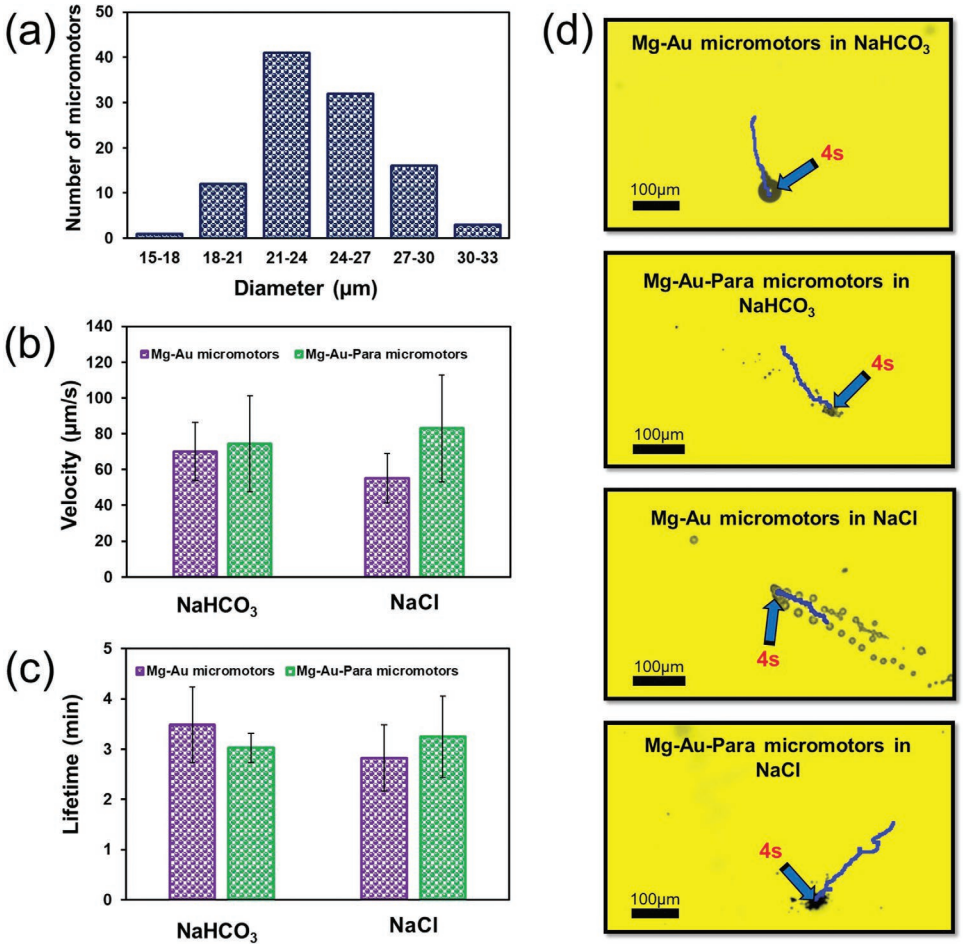

Figure 4. a) Size distribution of Mg-Au-MMs. b) Average velocities, c) average lifetime, and d) time-lapse tracking images of Mg-Au and Mg-Au-Para-MMs in $NaHCO_3$ and NaCl fuels, separately.

feature. The moving MC could in this way distribute the MM over a larger local area.

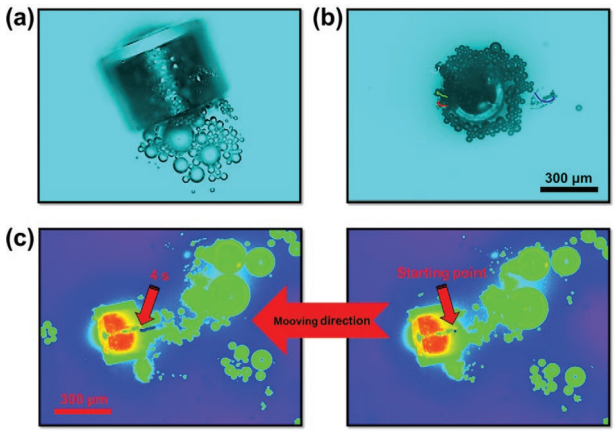

Figure 5. Optical images of Mg-Au-Para-MM-MCs submerged in fuel. a) Side view of MC bubbling during MM release, and b) top view of MC bubbling during MM release and tracking of a MM after it has exited the MC. c) Time-lapse tracking images of Mg-Au-Para-MM-MC in 2 M NaCl and 0.34 wt% Triton X-100.

We next turned our attention to examining the drug release from the cascade microdevices, and an in vitro drug release study was conducted using a μDISS profiler (**Figure 6**a). Due to size variations between the Mg-microparticles, it is roughly predicted the exact amount of drug on every MM (≈ 0.327 ng) and thus in every MC (≈0.288 μg). Drug loading calculation is provided in Supporting Information. MCs were loaded with pure paracetamol to serve as a control experiment (see Figure S3, Supporting Information). The first release study we performed was from Mg-Au-Para-MM and paracetamol powder-loaded MCs coated with 20 μm thick Eudragit L100 polymer at pH 7.4 (Figure 6b) and pH 2.5 (Figure 6c). MCs have been studied in our group during the last few years. Based on our knowledge and experience, 20 μm thickness of Eudragit L100 should prevent a premature cargo release. As Eudragit L100 dissolves at pH > 6, we expected the release of the drug to be slower in pH 2.5 compared to pH 7.4. As seen in Figure 6b,c, the powder drug indeed released significantly slower in the lower pH (76% at pH 7.4 and 16% at pH 2.5 in 30 min). However, when comparing the release of the drug from the Mg-Au-Para-MM-MCs (red line) to the control experiment (blue line), an interesting observation can be made. At pH 7.4, both releases follow a similar pattern of a relatively fast and early release (Mg-Au-Para-MM-MC

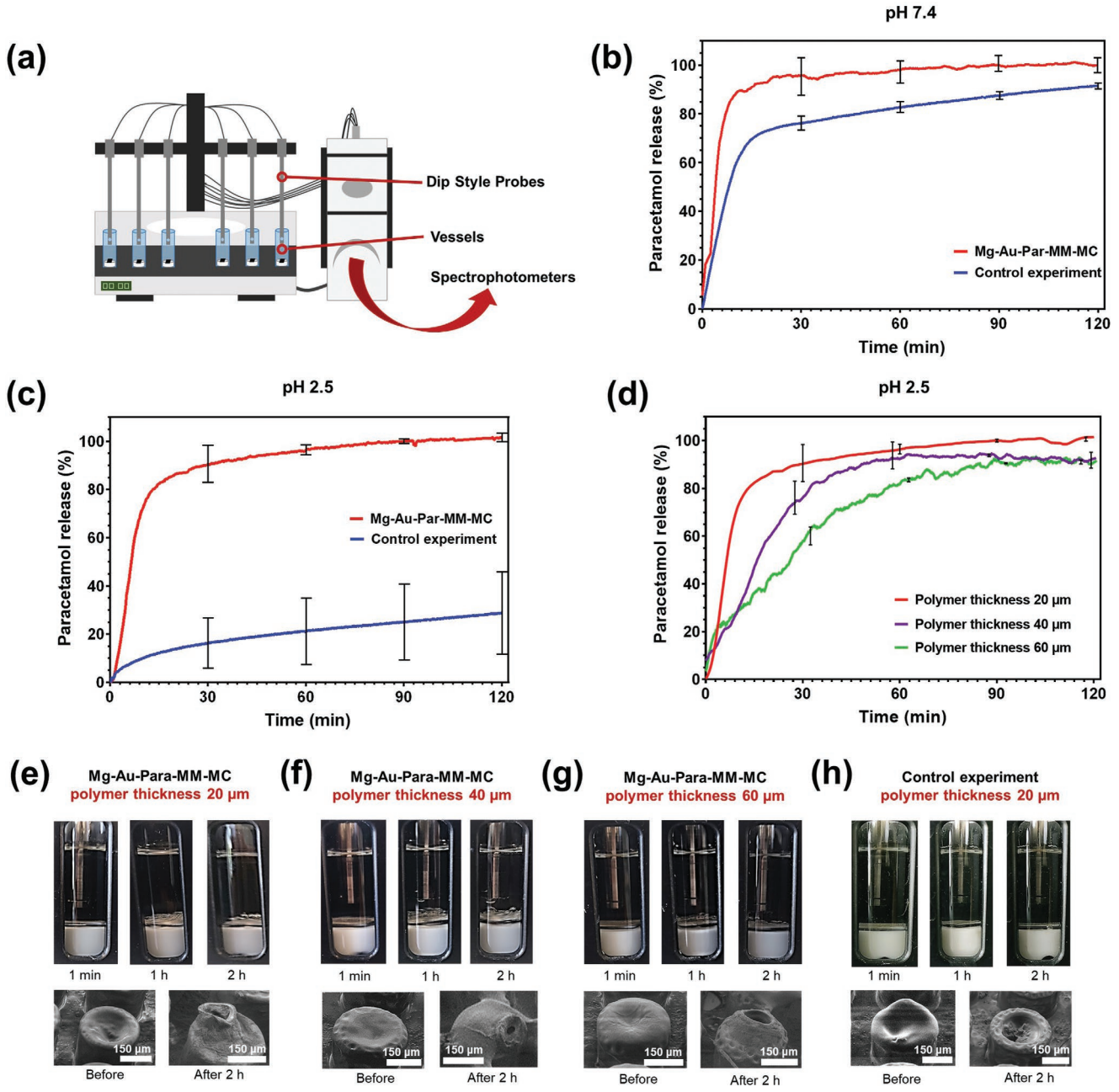

Figure 6. a) Schematic overview of in vitro study using µDISS equipment. Paracetamol release profiles over 2 h obtained from MC chips filled with Mg-Au-Para-MMs (red lines) and MC chips filled with bare paracetamol (control experiment, blue lines) at b) pH 7.4 (Eudragit L100 polymer thickness 20 µm), c) pH 2.5 (Eudragit L100 polymer thickness 20 µm), d) pH 2.5 (Eudragit L100 polymer thickness 20 µm [red line], 40 µm [purple line], and 60 µm [green line]). Data are presented as mean ± STD ($n = 3$). e–g) Bubble formation of MMs and SEM images before and 2 h after started in vitro experiment. MCs filled with Mg-Au-Para-MMs and coated with e) 20 µm, f) 40 µm, and g) 60 µm thick polymer coating. h) Absence of bubbles for performed control experiment followed by SEM images before and after an experiment.

releases 95% of paracetamol in 30 min and for the same time, MC loaded with bare paracetamol powder releases 76%), which slowly decreases over time. However, when comparing the results at pH 2.5, one can clearly see that the Mg-Au-Para-MM-MCs releases drug significantly faster (90%) than the one in the control experiment (16%). A possible explanation for this phenomenon is that when the MMs are in contact with acid media, bubble generation will start (Figure 6e). If a hole is formed in the Mg-Au-Para-MM-MCs coating or if the coating is permeable to liquid, the MMs would react to the acidic fuel entering the MC and propel themselves by producing bubbles. This MM movement would result in damaging the coating and speeding up the drug dissolution compared to the control, where no bubble generation is formed (Figure 6e,h). Moreover, due to the bubble formation within the MC, even if the MMs can pierce the coating themselves, increased pressure would be formed

within the MC which would result in "popping off" the coating of the MCs.

To see if it was possible to delay the drug release of the Mg-Au-Par MM loaded MCs at pH 2.5, the Eudragit coating thickness was increased to 40 and 60 μm by increasing the number of loops during spray coating. A thicker coating layer should lead to a further delay in the release of the drug.[49] As seen in Figure 6d, Eudragit L100 coating thickness of 40 and 60 μm, resulted in a significant delay in drug release compared to 20 μm. In detail, after 30 min, the Mg-Au-Para-MM-MCs coated with 20 μm thick Eudragit L100 had released 90% of its drug, the Mg-Au-Para-MM-MCs coated with 40 μm thick Eudragit L100 coated sample had released 75% of its drug, and the Mg-Au-Para-MM-MCs coated with 60 μm thick Eudragit L100 had released 60% of its drug. However, despite the significantly thicker polymeric coating, the pressure build-up, caused by the MMs, still results in damaging the polymeric coating and releasing the drug prematurely Figure 6f,g. The resulting MC structure to some degree resembles an erupted volcano.

Based on the obtained results, the release of bare paracetamol solution occurred as expected, being influenced only by the dissolution speed of the polymer. On the other hand, the release of drug from Mg-Au-Para-MM-MCs, gave us interesting data on how interactions with the MMs and their bubble formation can influence solvent penetration into the MCs and coating durability. For this technology to be applied to future commercially viable products, this is a challenge to overcome. One choice is the use of a thicker layer of enteric coating to ensure that the release of the MMs does not occur prematurely. The use of a different and slower dissolving coating altogether can also be considered. Alternatively, one can use capsules where the Mg-Au-Para-MM-MCs would be dispersed and protected before their desired release. This would present a new three-level cascade device that first offers delivery to specific parts of the GI tract by enteric coating of the larger capsule. Next, mucus embedment and unidirectional release is provided by MCs and finally complete mucus penetration is ensured by the MMs.

While multiple MM motion studies have been tested in various media, their motion has never previously been studied in porcine mucus. Assessment of MMs motion in mucus, therefore, is a crucial part in determining their effectiveness as drug carriers within the body. Thus, we performed an ex vivo study within porcine mucosa (**Figure 7**a), to test our system. We wanted to determine whether the presence of the mucus would affect the release of MMs from the MCs. For this study we observed Mg-Au-Par-MM-MCs coated with Kollicoat protect in 20 μL porcine mucus alongside 2 μL of 3 M NaCl and 2 μL 1 wt% Triton X-100. Kollicoat protect was chosen as the polymer coating in this experiment because of its ability to be released immediately, independent of pH value. 1 min after contact with fuel, the MCs started to produce bubbles (Figure 7b), showing that the coating had dissolved, and the media had access into the MCs cavity. Next, we investigated whether MMs left the MCs by taking images of Mg-Au-Para-MM-MCs at different time-points while they were being submerged within mucus. Figure 7d shows the MC 1 min after submersion into the mucus when it was full of MMs and intense bubbling started occurring. 5 min after submersion there is a decrease of material within the cavity and also a decrease in bubbling. 25 min after submersion in mucus, low amount of bubble formation occurs and a significant decrease in material can be seen within the MC. While not all the MMs succeeded in leaving the MC, this could be explained by the static nature of the experiment. Under real life conditions, the movement that MCs would experience within the GIT could assist all MMs in releasing from the MCs. Subsequently, we studied the motion of Mg-Au-Par-MM within porcine mucus. Their self-propulsion was observed and subsequently their velocity was calculated. The same was performed with MMs released from MCs coated with Kollicoat protect. Both systems showed propulsion within the mucus (Figure 7c). The MMs that were stored in MCs reached an impressive average velocity of 30.1 ± 7.9 μm s^{-1}, while the MMs stored in EtOH had a velocity of 11.5 ± 6.6 μm s^{-1} (Figure 7C). These velocities are lower compared to average velocities of MMs in the fuels (NaCl or $NaHCO_3$) without mucus. This was expected due to the increase in viscosity. To substantiate whether the velocity is affected by storing the MMs in MCs compared to free MMs (stored in EtOH), we performed a one-tailed *t*-test to compare the average velocities. A significant statistical difference was found when using a significance level of $p < 0.05$ ($p = 0.0003$). Therefore, we conclude that storing MMs in MCs can be beneficial for increasing their velocity. Furthermore, we observed a higher percentage of MMs being able to propel themselves when coming from MCs than the free ones. It could be due to the protection provided by the coated MCs that minimizes the chance of a propulsion-inhibiting passivation layer to appear. Tracking of Mg-Au-Par-MM movement in the mucus at different time points is presented in Figure 7e. Moreover, unlike the motion study experiments in less viscous fuels, MMs showed an increased tendency to follow a linear trajectory in porcine mucosa, which was expected according to the literature.[66]

3. Conclusion

In this study, we have explored cascade drug delivery microdevices comprised of MMs and MCs and have investigated their ability to deliver a model drug and move through porcine mucosa. Aspects of the characterization and morphology of both MCs and MMs have been analytically evaluated. CARS microscopy has been used to visualize drug distribution across carrier MCs as it does not require labeling (due to its ability to use its target's intrinsic vibrational signature to produce a selective signal) and the process is highly non-destructive and non-invasive. We have proved the self-propulsion of the biocompatible and non-toxic Mg-Au-Para-MMs in NaCl, $NaHCO_3$, and in mucus, separately. Next, Mg-Au-Para-MMs were successfully loaded in cylindrical MCs and protected with the pH-sensitive polymer Eudragit L100. Besides the good protection of the drug, MCs improve the retention, GIT localization, and unidirectional release of the drug. Furthermore, we have demonstrated that MCs do not compromise the excellent propulsion of Mg-Au-Para-MMs in contact with fuel. On the contrary, we have observed additional movement of the MCs filled with MMs due to the reaction of the Mg part of MMs with the fuel. This could potentially be explored as a means to ensure further

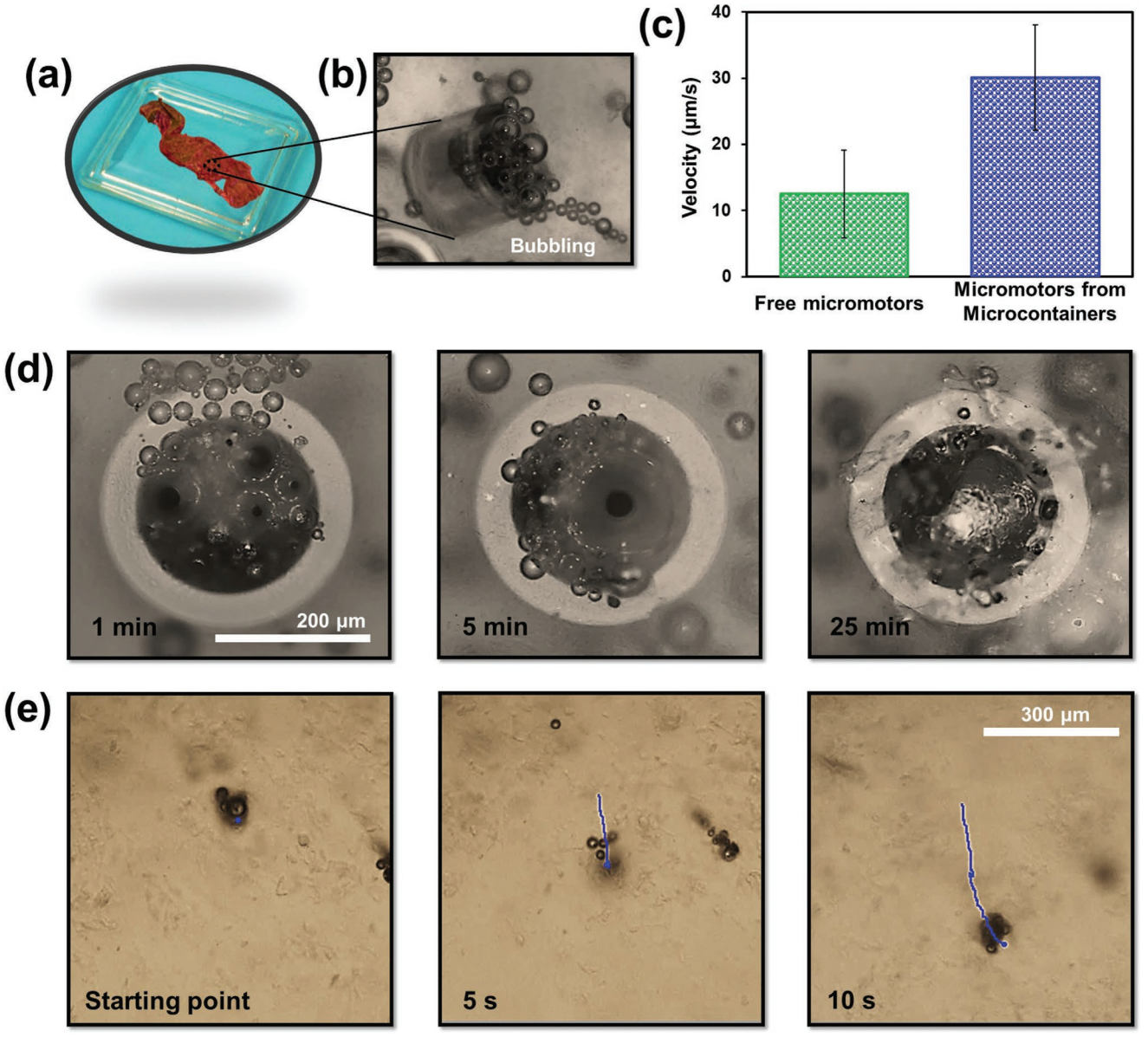

Figure 7. a) Dissected porcine GIT before mucus extraction. b) The Mg-Au-Para-MM-MC releases a vast number of bubbles from its cavity. c) Average velocities of Mg-Au-Para-MMs in mucus that were previously stored in EtOH and Mg-Au-Para-MMs in mucus that were stored in MCs coated with Kollicoat protect. Error bars are standard deviation. d) The Mg-Au-Para-MM-MC after 1, 5, and 25 min of being submerged within mucus. e) Tracking of the Mg-Au-Par-MM movement in the mucus at different time points. NaCl and Triton X-100 are added to the sample.

mucus embedment. Most significantly, ex vivo studies demonstrated that the MCs enable faster velocity of MMs after they release in a porcine mucosa compared to the velocity of free MMs placed in a porcine mucosa. Through in vitro studies, we verified that the MCs were able to 1) efficiently carry the drug, 2) ensure a quick polymer lid dissolution, and 3) provide fast paracetamol release in a neutral (pH = 7.4) environment and a delayed release in an acidic (pH = 2.5) environment. However, an unexpectedly fast release occurred in low pH environment, which may be due to the MMs "erupting" through the coating, resulting in its destruction. This challenge has been addressed by increasing the thickness of Eudragit L100 polymer coating to prevent premature drug release. In the future, we should explore the MCs encapsulation together with loaded MMs using different capsules or tablets that could consist of various formulations depending on the application. The use of different and slower dissolving polymers should also be considered.

4. Experimental Section

MMs Fabrication: Mg microparticles (catalogue no. FMW20, Tangshan Weihao Mg Powder Co.; 20 ± 5 µm) were used as the core of the Janus MMs. First, 2 mg of Mg powder was weighted on an analytical microbalance (Mettler Toledo, XPE26) and afterward cleaned in 1 mL of Acetone (VWR, USA). To guarantee the removal of the $Mg(OH)_2$ passivation layer, three rounds of washing steps were performed. Each round consisted of 10 min of sonication in a 2210 DTH

Branson ultrasonic cleaner (Branson Ultrasonics, USA), 10 min of centrifugation in an Eppendorf microcentrifuge (Eppendorf, Germany) at 10 000 rpm, removal of the supernatant without disturbing the Mg pellet, and last, adding 1 mL of acetone for the first two rounds of washing while 1 mL of absolute ethanol (VWR, USA) after the final round. Subsequently, the Mg solution was placed on top of a 2-inch single-side-polished silicon wafer (Active Business Company GmbH, Germany) and left to dry at room temperature inside a fume hood. The Au layer was deposited using a 2-inch TORUS magnetron sputtering cathode (Kurt Lesker, Jefferson Hills, USA). It was run in direct current mode using an Au cathode target (99.9% purity) provided by the same company. The Ar gas pressure was set to 50 mTorr (6.7 Pa), and the magnetron discharge was sustained at 400 V for a discharge current of 200 mA. The desired 20 nm gold layer thickness was achieved after a deposition time of 25 s. At the end, Mg-Au-MMs were sonicated in an acetone to promote detachment from the silicon wafer and supernatant was removed.

Drug Coating: The paracetamol (A5000, Sigma-Aldrich, USA) was dissolved in ethanol absolute solution (24 g L^{-1}), mixed with 10 mg of free Mg-Au-MMs and stirred for 18 h. Thereafter, the contents were transferred to Eppendorf tubes, centrifuged at 10 000 rpm for 10 min, followed by removal of the supernatant. Last, 200 µL of ethanol absolute was added to disperse the MMs, resulting in the final Mg-Au-Para-MMs suspension.

Fabrication, Loading, and Spray Coating of MCs: The MCs were fabricated in the negative photoresist SU-8 (SU-8 grade 2035 and 2075 Kayaku Advanced Materials, MA, USA) using a dual UV exposure scheme in which the impermeable bottom and sidewalls were defined in two successive steps. The fabrication method and explicit details were outlined in numerous publications.[67]

The MCs were fabricated on a 4-inch single-side-polished silicon substrate (Siegert wafer GmbH, Aachen, Germany) onto which a thin layer composed of 5 nm Ti and 20 nm Au was deposited by means of physical vapor deposition (Temescal FC-2000, Ferrotec Corporation, USA) to promote detachment of the individual MCs after MM loading and lid coating. The substrate was cut into chips of 12.8×12.8 mm^2, each having 625 MCs in a well-defined 25×25 2D array. The exact topography of the MCs was characterized by optical microscopy (Nikon Eclipse L200, Nikon Metrology, Japan) and vertical scanning interferometry (PLu Neox 3D Optical Profiler, Sensofar Metrology, Spain) The exact size of each MC was determined in advance with an average inner diameter 230 µm, average outer diameter 330 µm, and overall height 240 µm.

The MCs were loaded with Mg-Au-Para-MMs using a PDMS (Sylgard 184; Dow Corning, MI, USA shadow) mask.[54] The PDMS mask was used to avoid loading MMs in the voids between MCs thereby only targeting the concave cylindrical compartments of the MCs. Following this, 100 µL of the Mg-Au-Para-MM solution was pipetted onto each chip and said procedure was repeated until all containers were fully loaded. Next, the mask was gently removed by detaching it from the chip using tweezers. The loading of the pure paracetamol powder for in vitro study was performed using a nickel shadow mask applied on the top of the chip, again to cover voids between MCs.[68]

For the in vitro release studies, MCs loaded with Mg-Au-Para-MMs and MCs loaded with paracetamol powder (control sample) were sealed by ultrasonic spray coating (ExactaCoat system, Sono-Tek, Milton, NY, USA) of an isopropanol solution with 1% w/v Eudragit L100 (Evonik Industries AG, Germany) and 0.5% w/w of the liquid plasticizer dibutyl sebacate. Eudragit L100 was a 1:1 co-polymer consisting of methacrylic acid and methyl methacrylate. The spray coater was equipped with a microbore-fitted 120 kHz Vortex nozzle (Sono-Tek, Milton, NY, USA) and spray coating was performed using a generator power of 1.5 W, a hot plate temperature of 40 °C, and a cladding air pressure of 0.03 bar which was fed to the nozzle to sustain a circulating envelope for the atomized droplets. The liquid infusion rate was set to 1.5 mL min^{-1} and the nozzle was programmed to linearly move across samples with 150, 300, and 450 loops (1 loop = one linear passage), respectively. MCs used in the control experiment were coated with using 150 loops. The polymer thickness was measured on a planar reference substrate using an Alpha-Step IQ stylus profilometer (KLA-Tencor Corporation, USA).

To demonstrate the dynamic behavior of the MMs after they were released from the MCs, the MCs were sealed by spray coating a Milli-Q water (Merck Millipore, USA) solution with 1% w/v Kollicoat protect (BASF, Germany) polymer using the same coating protocol as outlined above. Kollicoat protect consisted of 55–65% polyvinyl alcohol (PVA)-polyethylene glycol graft co-polymer, 35–45% PVA, and 0.1–0.3% silicon dioxide. The infusion rate was reduced to 1 mL min^{-1} and a dwell time of 20 s was added between consecutive loops to ensure water evaporation. Each chip was coated with 225 loops. Coated MCs were submerged in an aqueous solution containing 2 M NaCl and 0.34 wt% Triton X-100 and later, short videos were taken.

Characterization: An AFEG 250 analytical SEM (FEI, USA) equipped with an EDX detector was used to collect SEM and EDX images of the produced MMs. SEM images of MCs before and after lid coating and before and after the in vitro study, were acquired using a tabletop SEM (TM3030 Plus, Hitachi High-Technologies Europe, Krefeld, Germany). Imaging and drug presence was confirmed using a Leica TCS SP8 CARS microscope (Leica, Germany) equipped with the CARS 2000S or CARS 1200S filter to gain more data regarding the drug loading. All the adjusted parameters for each separate experiment are shown in Table S1, Supporting Information.

The Raman shift was calculated using the following equation:

$$\text{Raman shift}\left[cm^{-1}\right] = \left(\frac{1}{\lambda p} - \frac{1}{\lambda s}\right) * 10^7 \quad (1)$$

In this equation, λp (nm) was the wavelength of the pump laser, while $\lambda s = 1032$ nm was the wavelength of the Stokes laser.

Motion Analysis: A Leica INM100 optical microscope (Leica, Germany) equipped with a Nikon DS-Fi2 digital sight camera (Nikon, Japan) and NIS Elements Software D version 4.20 (Nikon, Japan) was used to measure the size of Mg microparticles and record the motion of MMs. The Mg-Au-Para-MM-MCs were scraped off the silicon wafer/holding chip and mixed with a 2 M NaCl or 0.67 M NaHCO3 fuel, separately. Triton X-100 (Sigma-Aldrich, USA) was chosen as the best performing surfactant. Subsequently, videos of the moving MMs were recorded and then analyzed using ImageJ software. Individual MMs were tracked by applying manual tracking plugin in the ImageJ software. Averaged velocities and lifetime studies were measured from 20 recorded videos for each studied condition. The frame rate of the videos was 50 frames s^{-1}.

Data Analysis: Data analysis was carried out in Microsoft Excel (Microsoft Office Professional Plus 2016) and GraphPad Prism version 9.3.1 (GraphPad, USA). The dynamic MM behavior was quantified using ImageJ software, version 1.53k (National Institutes of Health, USA). Data were presented as mean ± standard deviation (STD). To determine the significance of the obtained data, a one-tailed *t*-test with a significance level of $p < 0.05$ was conducted.

In Vitro Studies with Mg-Au-Para-MMs: A µDISS Profiler (Pion, MA, USA) equipped with in situ UV probes was used to determine the release of paracetamol from MCs loaded with Mg-Au-Para-MMs. The release was measured in two different media consisting of phosphate buffered saline (PBS) adjusted to pH 7.5 and 2.5, which was similar to intestinal and gastric pH in fasted rats, respectively.[69] Paracetamol calibration curves were constructed for every channel by addition of different volumes of a stock solution in 10 mL of PBS adjusted to pH 7.5 and 2.5, separately. In situ fiber-optic probes with a path length of 1 mm were applied and the absorbance was measured in the range of 264–274 nm. For the release experiments, the chips were attached to cylindrical magnets, introduced into a sample vial and 10 mL of medium was added. UV measurements were carried out for 120 min for both media. All experiments were performed at 37 °C with 100 rpm and the path length of the in situ probes of 1 mm. Finally, the coated MC chips were placed on top of magnetic holders and 10 mL of the medium was added to each vessel when starting the experiment. The in situ UV probes detected the absorbance of released drug for a duration of 120 min. All experiments were performed in three replicates.

Ex Vivo Studies: The ability of MMs to propel themselves was evaluated in porcine small intestinal mucus (Department of Experimental

Medicine, University of Copenhagen, Denmark). The porcine intestine was dissected, and the mucus was gathered with a spoon and transferred to a plastic vial. Its pH was measured at 6.76 using a Seven2Go pH Meter (Mettler-Toledo, USA). The Mg-Au-Par MMs and the Kollicoat protect-coated Mg-Au-Para-MM-MCs were placed in 20 µL of porcine mucus by addition of 2 µL of 3 M NaCl and 2 µL 1 wt% Triton X-100. The experiment was observed via Leica INM100 optical microscope (Leica, Germany) equipped with a Nikon DS-Fi2 digital sight camera (Nikon, Japan). The NIS Elements software D version 4.20 (Nikon, Japan) was used to capture videos showing the MM propulsion.

Supporting Information

Supporting Information is available from the Wiley Online Library or from the author.

Acknowledgements

The authors would like to acknowledge the Danish National Research Foundation (DNRF122) and Villum Fonden (Grant No. 9301) for intelligent drug delivery and sensing using microcontainers and nanomechanics (IDUN) and the Novo Nordisk Foundation (NNF17OC0026910). Additionally, the Carlsberg Foundation (CF19-0379) is acknowledged for the support regarding the coherent anti-Stokes Raman scattering (CARS) instrument.

Conflict of Interest

The authors declare no conflict of interest.

Data Availability Statement

The data that support the findings of this study are available in the Supporting Information of this article.

Keywords

coherent anti-Stokes Raman scattering imaging, microcontainers, micromotors, oral drug delivery, porcine mucosa

Received: October 14, 2022
Revised: December 7, 2022
Published online:

[1] K. L. Stoner, H. Harder, L. J. Fallowfield, V. A. Jenkins, *Patient* **2014**, *8*, 145.
[2] R. B. Shah, M. Patel, D. M. Maahs, V. N. Shah, *Int J Pharm Investig* **2016**, *6*, 1.
[3] P. J. Brooks, W. J. Spruill, R. C. Parish, D. A. Birchmore, *Arthritis Rheum.* **1990**, *33*, 91.
[4] J. F. Jin, L. L. Zhu, M. Chen, H. M. Xu, H. F. Wang, X. Q. Feng, X. P. Zhu, Q. Zhou, *Patient Prefer Adherence* **2015**, *9*, 923.
[5] B. Homayun, X. Lin, H. J. Choi, *Pharmaceutics* **2019**, *11*, 129.
[6] A. Paul, in *Introduction to Basics of Pharmacology and Toxicology*, Vol. *1*, Springer, Singapore **2019**, p. 81.
[7] S. Sadeghi, W. K. Lee, S. N. Kong, A. Shetty, C. L. Drum, *Pharmacol Res* **2020**, *158*, 104685.
[8] P. Tyagi, S. Pechenov, J. A. Subramony, *J. Controlled Release* **2018**, *287*, 167.
[9] A. M. dos Santos, S. G. Carvalho, A. B. Meneguin, R. M. Sábio, M. P. D. Gremião, M. Chorilli, *J. Controlled Release* **2021**, *334*, 353.
[10] D. Guimarães, A. Cavaco-Paulo, E. Nogueira, *Int. J. Pharm.* **2021**, *601*, 120571.
[11] L. H. Nielsen, S. S. Keller, A. Boisen, *Lab Chip* **2018**, *18*, 2348.
[12] L. Wang, H. Zhu, Y. Shi, Y. Ge, X. Feng, R. Liu, Y. Li, Y. Ma, L. Wang, *Nanoscale* **2018**, *10*, 11384.
[13] T. Maric, S. Atladóttir, L. H. E. Thamdrup, O. Ilchenko, M. Ghavami, A. Boisen, *Appl. Mater. Today* **2022**, *27*, 101418.
[14] C. Mazzoni, F. Tentor, S. A. Strindberg, L. H. Nielsen, S. S. Keller, T. S. Alstrøm, C. Gundlach, A. Müllertz, P. Marizza, A. Boisen, *J. Controlled Release* **2017**, *268*, 343.
[15] J. R. Jørgensen, L. H. E. Thamdrup, K. Kamguyan, L. H. Nielsen, H. M. Nielsen, A. Boisen, T. Rades, A. Müllertz, *J. Controlled Release* **2021**, *329*, 948.
[16] Z. Abid, S. Strindberg, M. M. Javed, C. Mazzoni, L. Vaut, L. H. Nielsen, C. Gundlach, R. S. Petersen, A. Müllertz, A. Boisen, S. S. Keller, *Lab Chip* **2019**, *19*, 2905.
[17] P. Marizza, S. S. Keller, A. Müllertz, A. Boisen, *J. Controlled Release* **2014**, *173*, 1.
[18] L. H. Nielsen, A. Melero, S. S. Keller, J. Jacobsen, T. Garrigues, T. Rades, A. Müllertz, A. Boisen, *Int. J. Pharm.* **2016**, *504*, 98.
[19] C. Mazzoni, L. H. Nielsen, in *Nanotechnology for Oral Drug Delivery: From Concept to Applications*, Academic Press, El **2020**, p. 285.
[20] S. E. Birk, J. A. J. Haagensen, H. K. Johansen, S. Molin, L. H. Nielsen, A. Boisen, *Adv. Healthcare Mater.* **2020**, *9*, 1901779.
[21] C. von Halling Laier, B. Gibson, J. A. S. Moreno, T. Rades, S. Hook, L. H. Nielsen, A. Boisen, *J. Controlled Release* **2019**, *294*, 91.
[22] X. Wei, M. Beltrán-Gastélum, E. Karshalev, B. E.-F. De Ávila, J. Zhou, D. Ran, P. Angsantikul, R. H. Fang, J. Wang, L. Zhang, *Nano Lett.* **2019**, *19*, 1914.
[23] L. Kong, A. Ambrosi, M. Z. M. Nasir, J. Guan, M. Pumera, *Adv. Funct. Mater.* **2019**, *29*, 1903872.
[24] J. Zhang, F. Mou, Z. Wu, S. Tang, H. Xie, M. You, X. Liang, L. Xu, J. Guan, *ACS Appl. Mater. Interfaces* **2019**, *11*, 16639.
[25] P. Mayorga-Burrezo, C. C. Mayorga-Martinez, M. Pumera, P. Mayorga-Burrezo, M. Pumera, C. C. Mayorga-Martinez, *Adv. Funct. Mater.* **2022**, *32*, 2106699.
[26] M. Zhou, Y. Xing, X. Li, X. Du, T. Xu, X. Zhang, M. Zhou, Y. Xing, X. Du, T. Xu, X. Zhang, X. Li, *Small* **2020**, *16*, 2003834.
[27] K. K. Dey, S. Bhandari, D. Bandyopadhyay, S. Basu, A. Chattopadhyay, *Small* **2013**, *9*, 1916.
[28] R. Dong, J. Li, I. Rozen, B. Ezhilan, T. Xu, C. Christianson, W. Gao, D. Saintillan, B. Ren, J. Wang, *Sci. Rep.* **2015**, *5*, 13226.
[29] V. V. Singh, B. Jurado-Sánchez, S. Sattayasamitsathit, J. Orozco, J. Li, M. Galarnyk, Y. Fedorak, J. Wang, *Adv. Funct. Mater.* **2015**, *25*, 2147.
[30] X. Xu, Z. Huo, J. Guo, H. Liu, X. Qi, Z. Wu, *Bio-Des. Manuf.* **2020**, *3*, 133.
[31] S. K. Lai, D. E. O'Hanlon, S. Harrold, S. T. Man, Y. Y. Wang, R. Cone, J. Hanes, *Proc. Natl. Acad. Sci. USA* **2007**, *104*, 1482.
[32] H. Choi, S. H. Jeong, T. Y. Kim, J. Yi, S. K. Hahn, *Bioact. Mater.* **2022**, *9*, 54.
[33] K. Yuan, B. Jurado-Sánchez, A. Escarpa, *Angew. Chem., Int. Ed.* **2021**, *60*, 4915.
[34] H. Eskandarloo, A. Kierulf, A. Abbaspourrad, *Nanoscale* **2017**, *9*, 12218.
[35] D. Yamamoto, A. Shioi, *KONA Powder Part. J.* **2015**, *32*, 2015005.
[36] F. Mou, X. Li, Q. Xie, J. Zhang, K. Xiong, L. Xu, J. Guan, *ACS Nano* **2020**, *14*, 406.
[37] F. Mou, Q. Xie, J. Liu, S. Che, L. Bahmane, M. You, J. Guan, *Natl. Sci. Rev.* **2021**, *8*, nwab066.
[38] K. Xiong, L. Xu, J. Lin, F. Mou, J. Guan, *Research* **2020**, *2020*, 4093732.

[39] X. Li, R. Wu, H. Chen, T. Li, H. Jiang, X. Xu, X. Tang, M. Wan, C. Mao, D. Shi, *ACS Appl. Mater. Interfaces* **2021**, *13*, 30930.
[40] T. Maric, M. Z. M. Nasir, M. Budanovic, O. Alduhaish, R. D. Webster, M. Pumera, *Appl. Mater. Today* **2020**, *20*, 100659.
[41] X. Zhang, W. Xie, H. Wang, Z. Zhang, *Chem. Commun.* **2021**, *57*, 3797.
[42] W. Cao, Y. Liu, P. Ran, J. He, S. Xie, J. Weng, X. Li, *ACS Appl. Mater. Interfaces* **2021**, *13*, 58411.
[43] S. Sanchez, L. Soler, J. Katuri, *Angew. Chem., Int. Ed.* **2015**, *54*, 1414.
[44] F. Mou, C. Chen, Q. Zhong, Y. Yin, H. Ma, J. Guan, *ACS Appl. Mater. Interfaces* **2014**, *6*, 9897.
[45] J. Lv, Y. Xing, T. Xu, X. Zhang, X. Du, *Appl. Mater. Today* **2021**, *23*, 101034.
[46] H. Wang, M. G. Potroz, J. A. Jackman, B. Khezri, T. Maric, N.-J. Cho, M. Pumera, H. Wang, B. Khezri, T. Maric, M. Pumera, M. G. Potroz, J. A. Jackman, N. Cho, *Adv. Funct. Mater.* **2017**, *27*, 1702338.
[47] B. E. F. De Ávila, P. Angsantikul, J. Li, M. A. Lopez-Ramirez, D. E. Ramírez-Herrera, S. Thamphiwatana, C. Chen, J. Delezuk, R. Samakapiruk, V. Ramez, L. Zhang, J. Wang, *Nat. Commun.* **2017**, *8*, 272.
[48] L. Cai, C. Zhao, H. Chen, L. Fan, Y. Zhao, X. Qian, R. Chai, L. Cai, C. Zhao, X. Qian, R. Chai, H. Chen, L. Fan, Y. Zhao, *Adv. Sci.* **2022**, *9*, 2103384.
[49] J. Li, S. Thamphiwatana, W. Liu, B. E.-F. de Ávila, P. Angsantikul, E. Sandraz, J. Wang, T. Xu, F. Soto, V. Ramez, X. Wang, W. Gao, L. Zhang, J. Wang, *ACS Nano* **2016**, *10*, 9536.
[50] M. D. Mosgaard, S. Strindberg, Z. Abid, R. S. Petersen, L. H. E. Thamdrup, A. J. Andersen, S. S. Keller, A. Müllertz, L. H. Nielsen, A. Boisen, *Int. J. Pharm.* **2019**, *570*, 118658.
[51] J. R. Jørgensen, F. Yu, R. Venkatasubramanian, L. H. Nielsen, H. M. Nielsen, A. Boisen, T. Rades, A. Müllertz, *Pharmaceutics* **2020**, *12*, 48.
[52] E. Karshalev, B. E.-F. De Ávila, M. Beltrán-Gastélum, P. Angsantikul, S. Tang, R. Mundaca-Uribe, F. Zhang, J. Zhao, L. Zhang, J. Wang, *ACS Nano* **2018**, *12*, 8397.
[53] L. Prescott, *Br. J. Clin. Pharmacol.* **1980**, *10*, 291S.
[54] K. Kamguyan, L. H. E. Thamdrup, L. Vaut, L. H. Nielsen, K. Zor, A. Boisen, *Biomed. Microdevices* **2020**, *22*, 35.
[55] K. V. Nemani, K. L. Moodie, J. B. Brennick, A. Su, B. Gimi, *Mater. Sci. Eng., C* **2013**, *33*, 4453.
[56] O. Charyeva, O. Dakischew, U. Sommer, C. Heiss, R. Schnettler, K. S. Lips, *J. Orthop. Traumatol.* **2016**, *17*, 63.
[57] E. C. Dreaden, M. A. Mackey, X. Huang, B. Kang, M. A. El-Sayed, *Chem. Soc. Rev.* **2011**, *40*, 3391.
[58] N. L. Rosi, C. A. Mirkin, *Chem. Rev.* **2005**, *105*, 1547.
[59] F. Zheng, P. Wang, Q. Du, Y. Chen, N. Liu, *Front. Chem.* **2019**, *7*, 232.
[60] L. Zhang, S. Granick, *Nano Lett.* **2006**, *6*, 694.
[61] J. R. Jørgensen, M. L. Jepsen, L. H. Nielsen, M. Dufva, H. M. Nielsen, T. Rades, A. Boisen, A. Müllertz, *Eur. J. Pharm. Biopharm.* **2019**, *143*, 98.
[62] C. Chen, E. Karshalev, J. Guan, J. Wang, *Small* **2018**, *14*, 1704252.
[63] Q. Chi, Z. Wang, F. Tian, J. You, S. Xu, *Micromachines* **2018**, *9*, 537.
[64] Y. Feng, X. Chang, H. Liu, Y. Hu, T. Li, L. Li, *Appl. Mater. Today* **2021**, *23*, 101026.
[65] F. Mou, C. Chen, H. Ma, Y. Yin, Q. Wu, J. Guan, *Angew. Chem., Int. Ed.* **2013**, *52*, 7208.
[66] G. Zhao, N. T. Nguyen, M. Pumera, *Nanoscale* **2013**, *5*, 7277.
[67] L. H. Nielsen, S. S. Keller, K. C. Gordon, A. Boisen, T. Rades, A. Müllertz, *Eur. J. Pharm. Biopharm.* **2012**, *81*, 418.
[68] Z. Abid, C. Gundlach, O. Durucan, C. von Halling Laier, L. H. Nielsen, A. Boisen, S. S. Keller, *Microelectron. Eng.* **2017**, *171*, 20.
[69] J. F. Christfort, S. Strindberg, J. Plum, J. Hall-Andersen, C. Janfelt, L. H. Nielsen, A. Müllertz, *Eur. J. Pharm. Biopharm.* **2019**, *142*, 307.